Supplementary Information

Rapid microwave synthesis of carbon-bridged Nb_2O_5 mesocrystals for high-energy and high-power sodium-ion capacitors

Yingjun Jiang, Songtao Guo, Yaqian Li, and Xianluo Hu*

Experimental Procedures

Materials synthesis for meso-Nb_2O_5@C

All chemicals were used without further purification. The synthesis process of meso-Nb_2O_5@C was illustrated by **Scheme 1**. Firstly, 5-mL oleic acid (OA) was added to 16 mL trioctylamine (TOA) and stirred to obtain a uniform mixed solution. Secondly, 0.4 g ammonium niobate (V) oxalate hydrate was added to the mixed solution and stirred at 50 °C for 5 h to obtain a homogeneous white solution. The obtained solution was transferred to the microwave reaction vessel and heated in a microwave synthesis system (Discover S-Class, CEM) at 160 °C for only 1 min. The intermediate was collected by centrifugation and then was heated in H_2/Ar atmosphere at 700 °C for 3 h at a heating rate of 2 °C min^{-1} (BTF-1200C-III, Anhui BEQ Equipment Technology CO., Ltd). The black meso-Nb_2O_5@C was obtained. The intermediates were washed several times by toluene for characterization. In addition, the optimized process has been provided as follows.

Materials synthesis for Nb_2O_5@C NPs

For comparison, commercial Nb_2O_5 nanoparticles with conformal carbon coating (denoted as Nb_2O_5@C NPs) were prepared according to our previous work.[1] Firstly, 0.3 g of commercial *T*-Nb_2O_5 nanoparticles were added to 6-mL absolute ethanol and then sonicated for 30 min to obtain a uniform dispersion. 90 μL of ionic liquid EMIm-dca was added to the stirring dispersion and the IL could physically adsorb on the surface of Nb_2O_5 nanoparticles. Then, the mixed dispersions were transferred to an oil bath at 90 °C for heating and stirring. A white intermediate was obtained by heating and evaporating ethanol and then heated in H_2/Ar atmosphere at 600 °C for 2 h with a heating rate of 2 °C min^{-1}. During the heat treatment, the ionic liquid adsorbed on the surface of Nb_2O_5 is pyrolyzed at high temperature to form conformal carbon coating to obtain Nb_2O_5@C NPs.

Materials characterization

The crystal structure of the sample was characterized by X-ray diffraction (XRD, Empyrean, PANalytical B.V.) and Raman spectrum with a wavelength of 532 nm (LabRAM HR800, Horiba JobinYvon). The morphology of the products was tested by scanning electron microscopy (SEM, Nova Nano SEM 450, FEI). At the same time, the microstructure was determined by transmission electron microscopy (TEM, Talos F200X, FEI). X-ray photoelectron spectroscopy (XPS, EscaLab Xi+, ThermoFischer) was used to characterize the elemental

information of the sample. The carbon content of the sample was detected by TGA (TGA8000, PerkinElmer) at a heating rate of 10 °C min^{-1} in air. The Brunauer–Emmett–Teller (BET) surface area and porosity were detected by nitrogen-sorption via a Micromeritics ASAP 2460 3.01 analyzer. The electrodes after cycles were cleaned with dimethyl carbonate for several times and then characterized by SEM and TEM.

Electrochemical measurements for the half cells

The electrochemical performance of the half-cell was tested in a CR2032-type coin cell which assembled in an argon-filled glove box (< 0.01 ppm of oxygen and water) with sodium foil as both counter electrode and reference electrode and glass fiber as separators. The working electrode is prepared as follows: Firstly, a slurry was obtained by mixing the active material, super P, Ketjen black, and polyacrylic acid in ethanol with the ratio of 7:1:1:1. Then, the slurry was homogeneously coated on Cu foil and dried in an oven at 80 °C. The mass loading of active materials is 0.6 ~ 0.8 mg cm^{-2}. The electrolyte is composed of 1 M $NaClO_4$ salt in ethylene carbonate and propylene carbonate (1:1 in vol : vol) with 5% fluoroethylene carbonate additive. The charge/discharge performance is carried out at various current densities (1 C = 200 mA g^{-1}) by LAND-V34 battery tester (Land Electronic Co., Ltd., Wuhan, China) with a potential range of 0.01–3.00 V (*vs.* Na/Na^+). The half-cell was activated for 15 cycles at a current density of 0.2 C before the rate test. Cyclic voltammetry (CV) and electrochemical impedance spectroscopy (EIS) were carried out by the electrochemical workstation (CHI 660E). The initial Coulombic efficiency is obtained by the ratio of the specific capacity for the charging process to the specific capacity for the discharging process in the first cycle.

Electrochemical measurements for the SICs

SICs was assembled by pre-sodiated meso-Nb_2O_5@C as a negative electrode and commercial activated carbon (YP-80F, Kuraray) as a positive electrode. The pre-sodiated meso-Nb_2O_5@C was prepared by activated at 0.2 C for 3 cycles and then discharged to 0.01 V (vs. Na/Na^+). The positive electrode is made by homogenously mixing AC, Super P, and polyvinylidene fluoride (PVDF) in N-methylpyrrolidone (NMP) in the ratio of 8:1:1. The electrochemical performance of all sodium-ion capacitors was tested by an electrochemistry workstation (CHI 660E). All current densities are based on the total mass of negative and positive active materials for all electrochemical tests for SICs. The voltage of this SIC is 0–3.9 V. The specific capacitance (F g^{-1}), energy density (Wh kg^{-1}), and power density (W kg^{-1}) of the whole device are calculated by the following formula:[2,3]

$$C = (I \times t) / (m \times (V_{max} - V_{min})) \quad (1)$$

$$E = (I \times t \times (V_{max} - V_{min})) / (2 \times 3.6 \times m) \quad (2)$$

$$P = 3600 \times E / t \quad (3)$$

Where I is the charge/discharge current (A), V_{max} and V_{min} are voltages (V) at the beginning and end of the discharge process, t is the discharge time (s), m is the total mass of active materials on both positive and negative electrodes (g).

Calculation of Sodium-ion Diffusion Kinetics for GITT

$$D_{Na} = 4 \times (m_B \times V_M \times \Delta E_S)^2 / (\pi \times \tau \times M_B \times S \times \Delta E_\tau)^2 \quad (4)$$

Where D_{Na} is the sodium ion diffusion coefficient. τ is the relaxation time. V_M is the molar volume. M_B is the molar mass. m_B is the mass of active materials in the electrode. S represents the area of the electrode. ΔE_S is the steady potential difference in the plateau region, while ΔE_τ is the voltage drop between beginning state and steady state. And Then, the square value of the ratio of ΔE_S and ΔE_τ has a linear relationship with sodium ion diffusion coefficient.

The optimization process for meso-Nb_2O_5@C

(1) Different microwave reaction time

Table S1 shows the experiment details to study the effects of different microwave reaction times (1, 10, 30 min) on the physicochemical properties of the products. The related characterization results are shown in **Fig. S1**, **S2**, **S8**, and **S11**, which also confirms that the physicochemical properties (like morphology, specific surface area, and pore distribution) could be tuned. The microwave reaction time has a negligible effect on the crystalline structure (**Fig. S1a**) and carbon content (**Fig. S1b**), which is collaborated to the formation mechanism of mesocrystals. According to the SEM images (**Fig. S2**), the Sample-1 min shows a nanorod-like morphology. With the time increases, the nanorod-like morphology is broken owing to the crystal growth. Furthermore, the Sample-1 min has some other similar physicochemical properties to Nb_2O_5@C NPs like specific surface area (**Table S2**), pore distribution (**Fig. S11b**), and carbon content (**Fig. S8**). In summary, the optimal microwave reaction time is 1 min.

(2) Different Nb^{5+} source concentrations

The experimental conditions are shown in **Table S3**. According to **Fig. S3a**, the concentration of the Nb^{5+} source does not affect the crystal structure of the product but has a certain effect on the morphology. The rod-like structure cannot be obtained with a low Nb^{5+} concentration (**Fig. S4a** and **f**), which may be related to the excessive OA molecules in the reaction solution. There is a strong hydrogen bond between excessive OA and Nb-O nano-units (coordinated by OA molecules) because of carboxylic groups in OA molecules, and then resulting in aggregation. Meanwhile, there are many nanoparticles expected for the nanorods (**Fig. S4e** and **j**) with a high concentration of Nb^{5+} source. It is speculated that those nanoparticles may be related to the insufficient OA molecules for the coordination of Nb-O units. This phenomenon strongly confirms the formation mechanism of mesocrystals again. In a word, 0.4 g Nb^{5+} source has been chosen as the optimized condition.

(3) Different ratios of OA to TOA

According to previous reports on materials synthesis,[4,5] we optimized the proportion of the OA/TOA solvents as shown in **Table S4**. There is a negligible effect on the crystal structure for T-Nb_2O_5 (**Fig. S3b**), but a great influence on the morphology of the products (**Fig.**

S5) in different proportions of the OA/TOA solvents. Here, we choose the proportion of OA : TOA = 5 :16 (vol / vol) as the optimal condition.

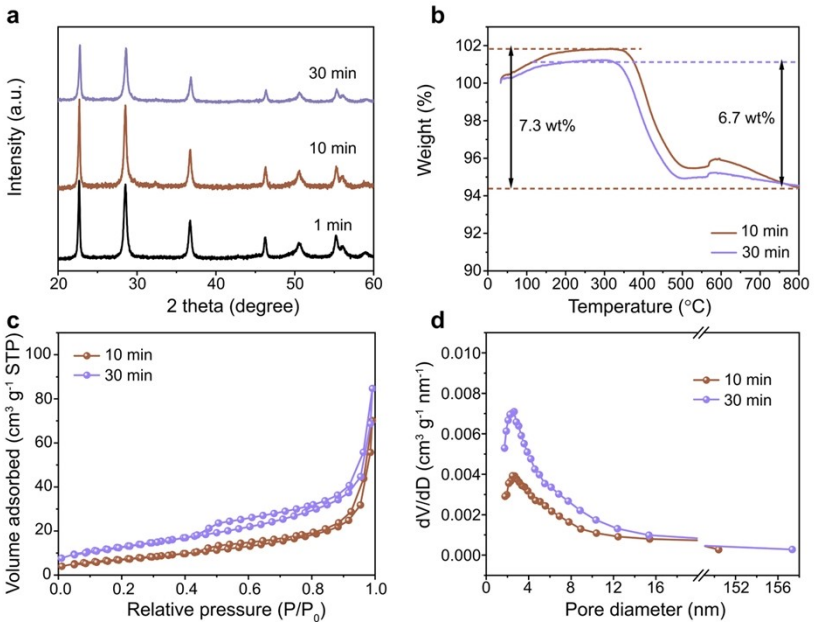

Fig. S1 Materials characterization for the samples with different microwave reaction time: (a) XRD patterns; (b) TG; (c) Nitrogen adsorption and desorption isotherm and (d) the corresponding pore size distribution.

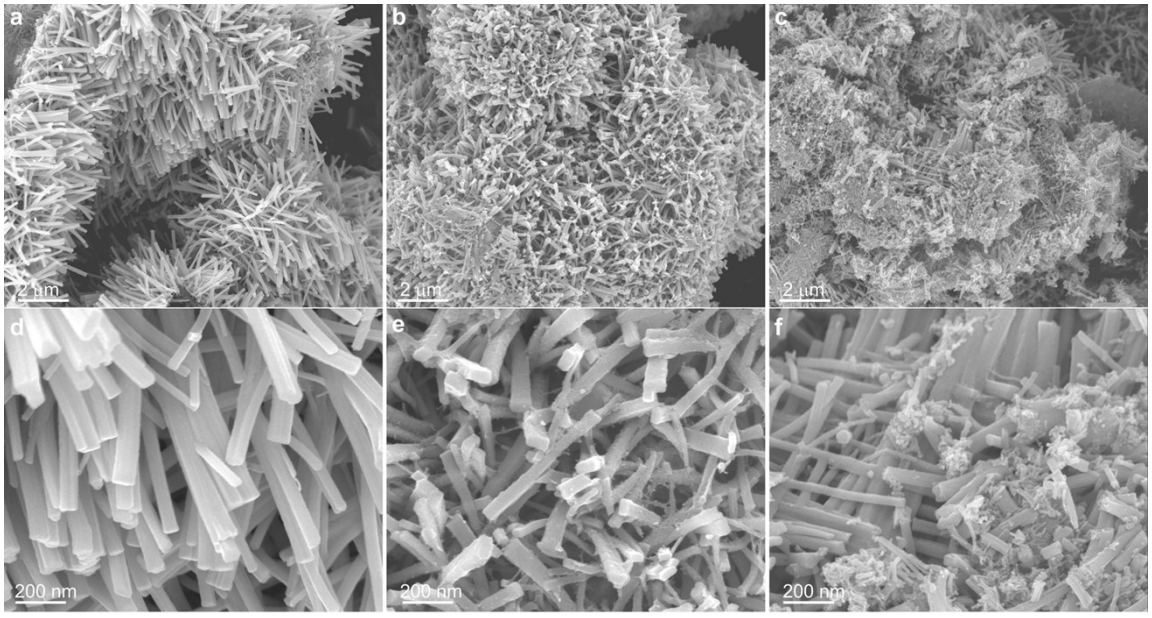

Fig. S2 SEM images for the samples at different microwave reaction time: (a, d) 1 min; (b, e) 10 min; (c, f) 30 min.

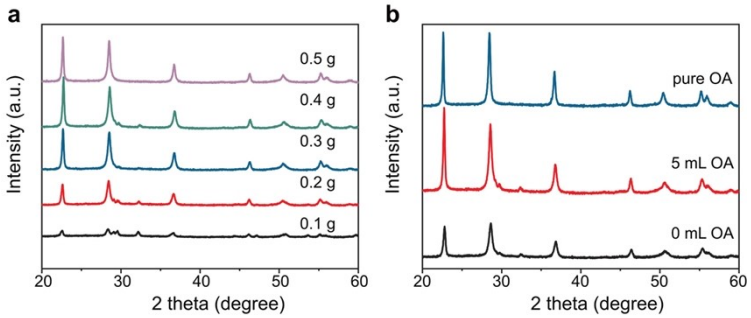

Fig. S3 XRD patterns for the products at different conditions: (a) different concentration for the Nb source for precursor solution; (b) different OA and TOA ratios for the precursor solution.

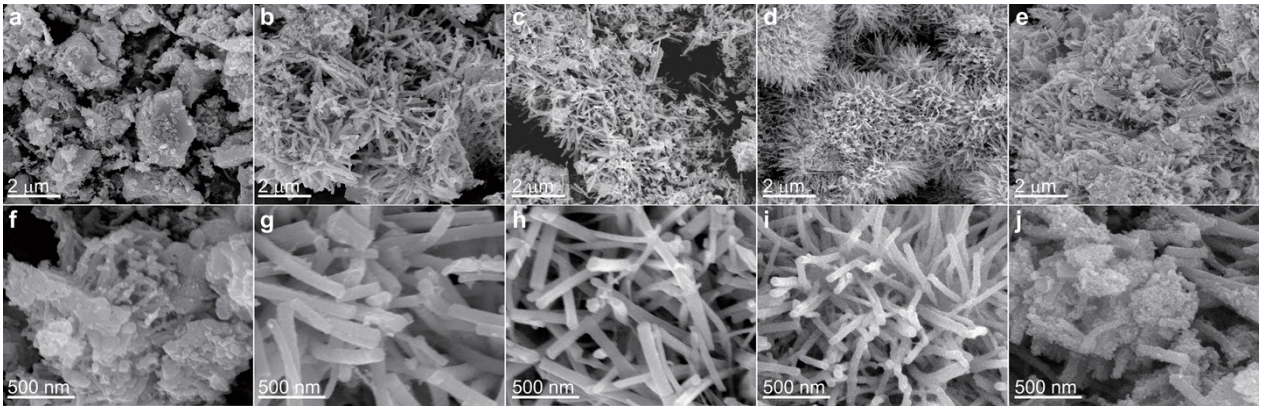

Fig. S4 Different concentrations for Nb source for precursor solution: (a, f) 0.1 g; (b, g) 0.2 g; (c, h) 0.3 g; (d, i) 0.4 g; (e, j) 0.5 g.

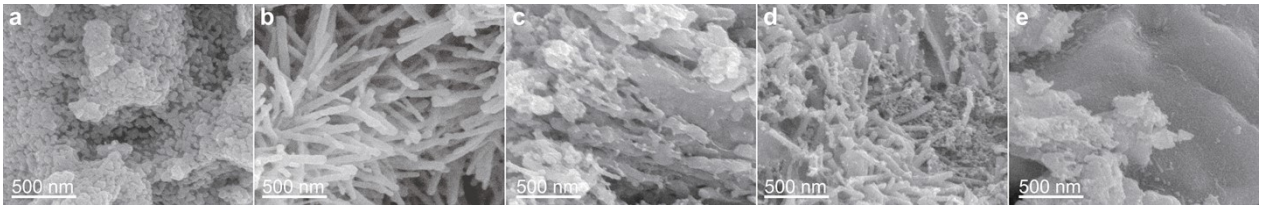

Fig. S5 Different OA volumes in the precursor solutions: (a) 0 mL OA; (b) 5 mL OA; (c) 16 mL OA; (d) 21 mL OA; (e) pure OA.

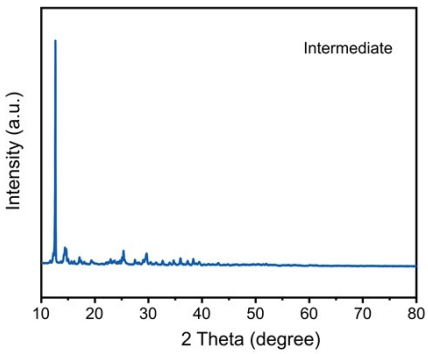

Fig. S6 XRD result for the intermediate.

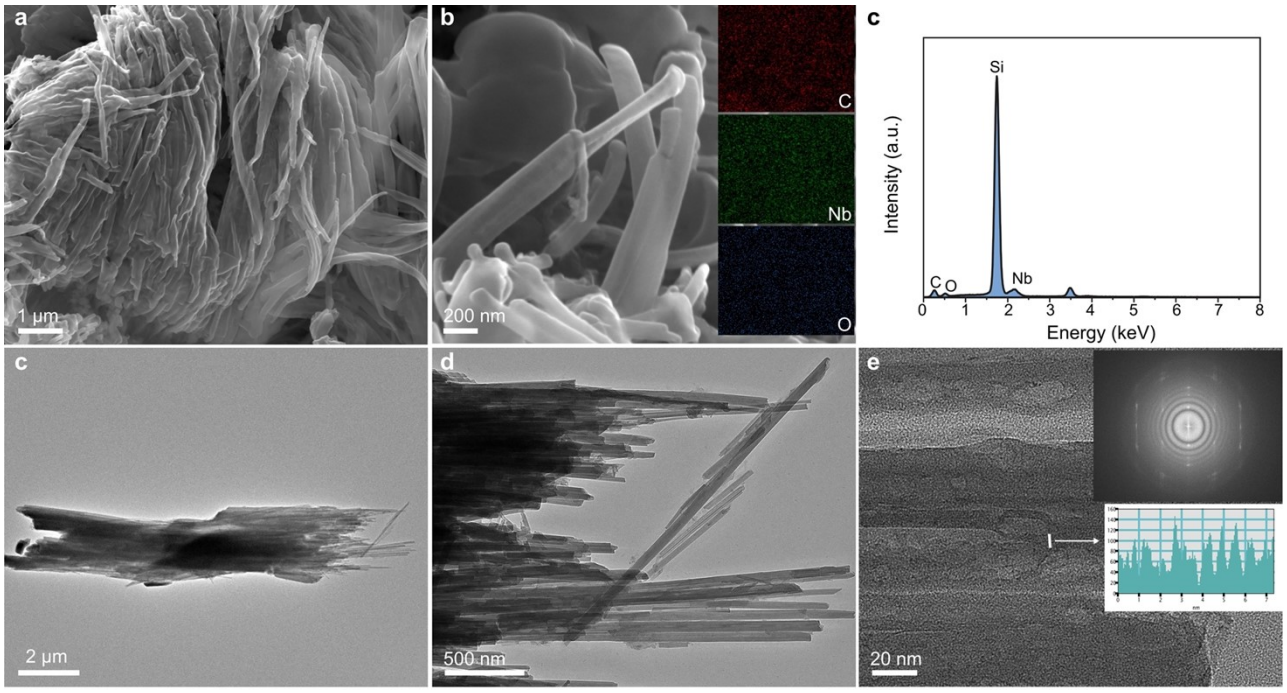

Fig. S7 SEM images (a, b), EDX result (c), and element mapping (inserted in b) for intermediate. TEM images (d-f) for intermediate, the inserted image corresponds to the SAED pattern.

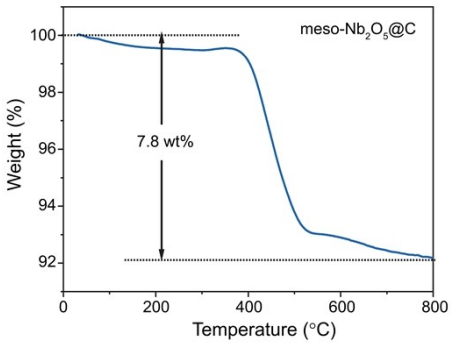

Fig. S8 TG for meso-Nb_2O_5@C.

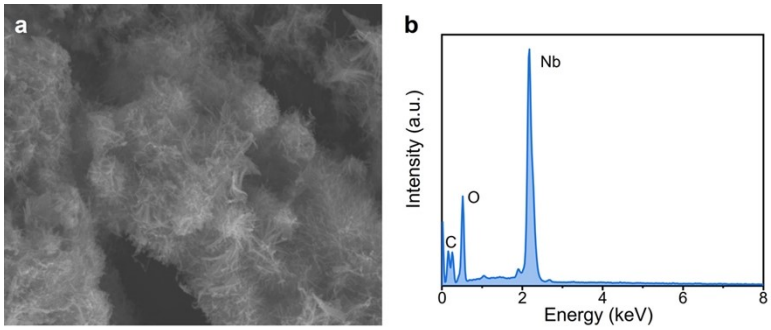

Fig. S9 SEM images for meso-Nb_2O_5@C (a) and corresponding EDS images.

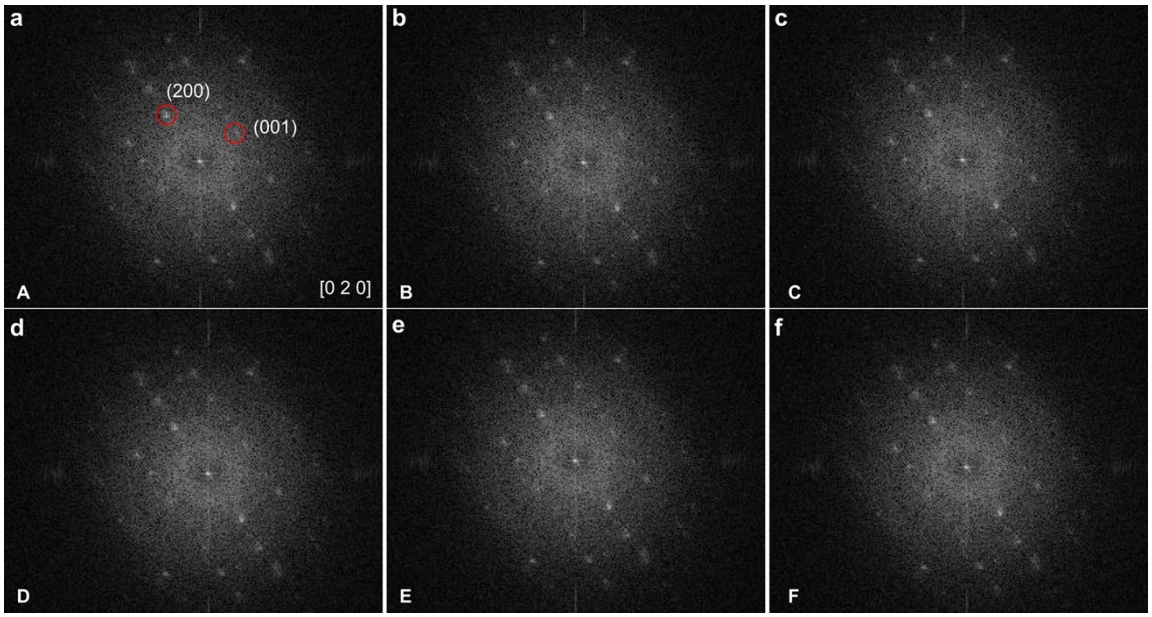

Fig. S10 FFT patterns of different areas corresponding to the regions shown in Fig. 2e: (a) A, (b) B, (c) C, (d) D, (e) E, (f) F region.

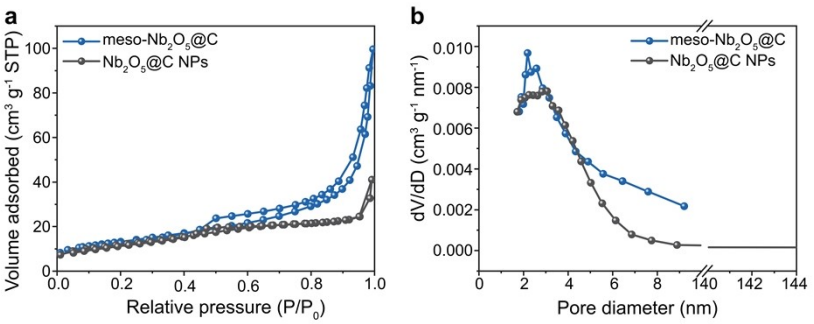

Fig. S11 (a) Nitrogen adsorption and desorption isotherm and (b) the corresponding BJH pore size distribution for meso-Nb_2O_5@C and Nb_2O_5@C NPs.

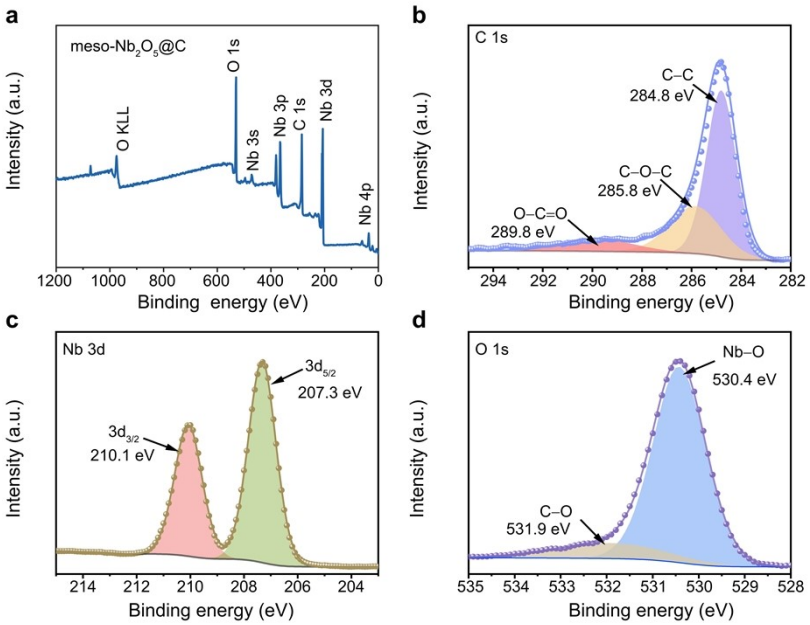

Fig. S12 XPS results for meso-Nb_2O_5@C: (a) XPS spectra ; high-resolution C 1s (b), Nb 3d (c) and O 1s (d) spectra.

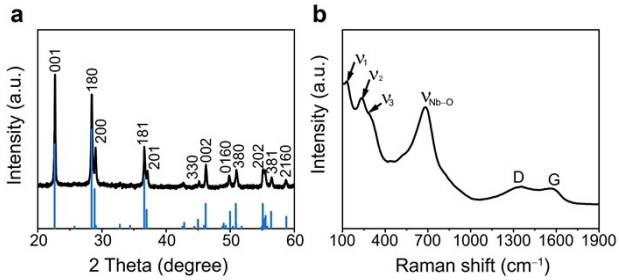

Fig. S13 (a) XRD pattern and (b) Raman spectrum for Nb_2O_5@C NPs.

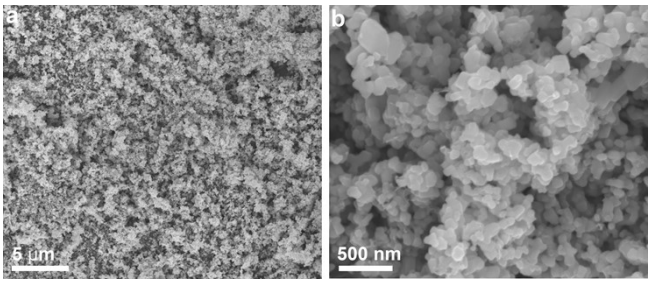

Fig. S14 SEM images for Nb_2O_5@C NPs.

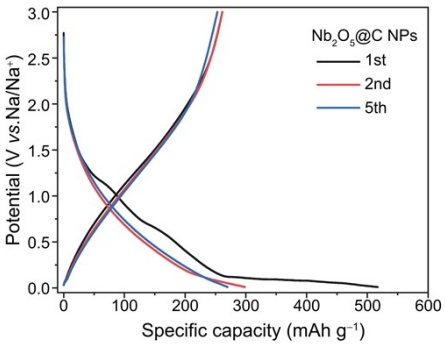

Fig. S15 Galvanostatic discharge/charge voltage profiles for Nb_2O_5@C NPs with different cycles at 0.2 C.

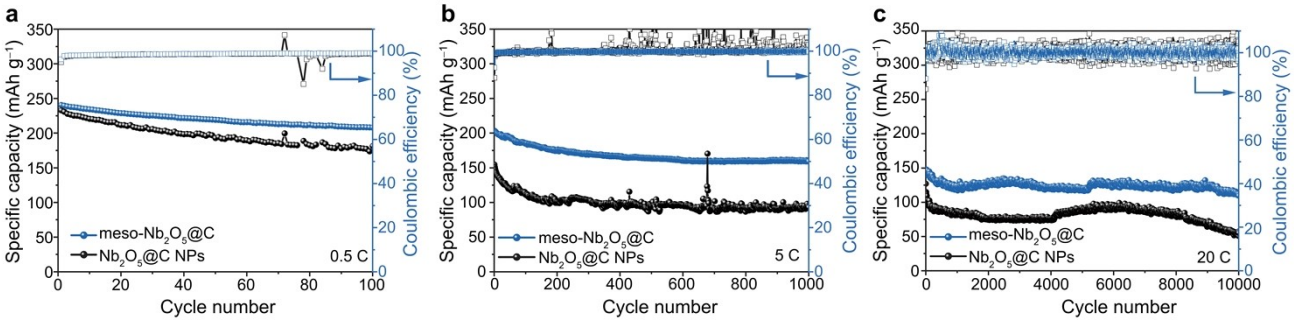

Fig. S16 Cycling performance at the current density of 0.5 C (a), 5 C (b) and 20 C (c) for meso-Nb_2O_5@C and Nb_2O_5@C NPs.

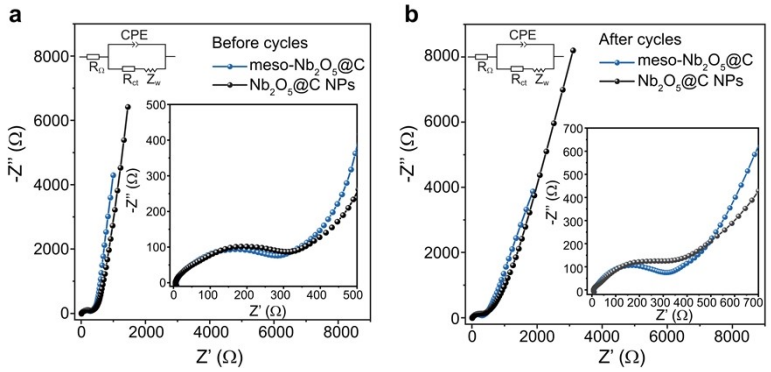

Fig. S17 (a) Nyquist plots of meso-Nb_2O_5@C and Nb_2O_5@C NPs before (a) and after (b) 1,000 cycles at 5 C.

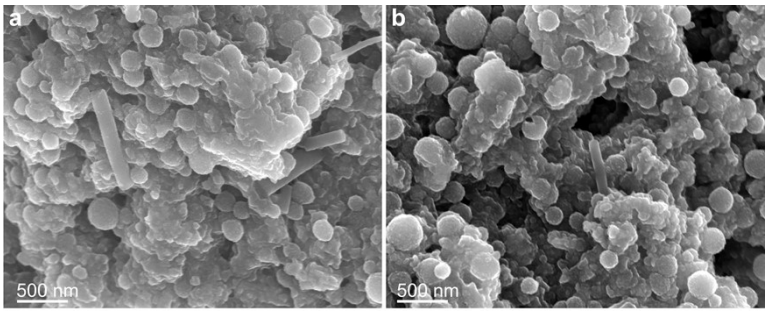

Fig. S18 SEM images for the meso-Nb_2O_5@C electrode from different regions: (a, b) at 20 C after 10,000 charge-discharge cycles.

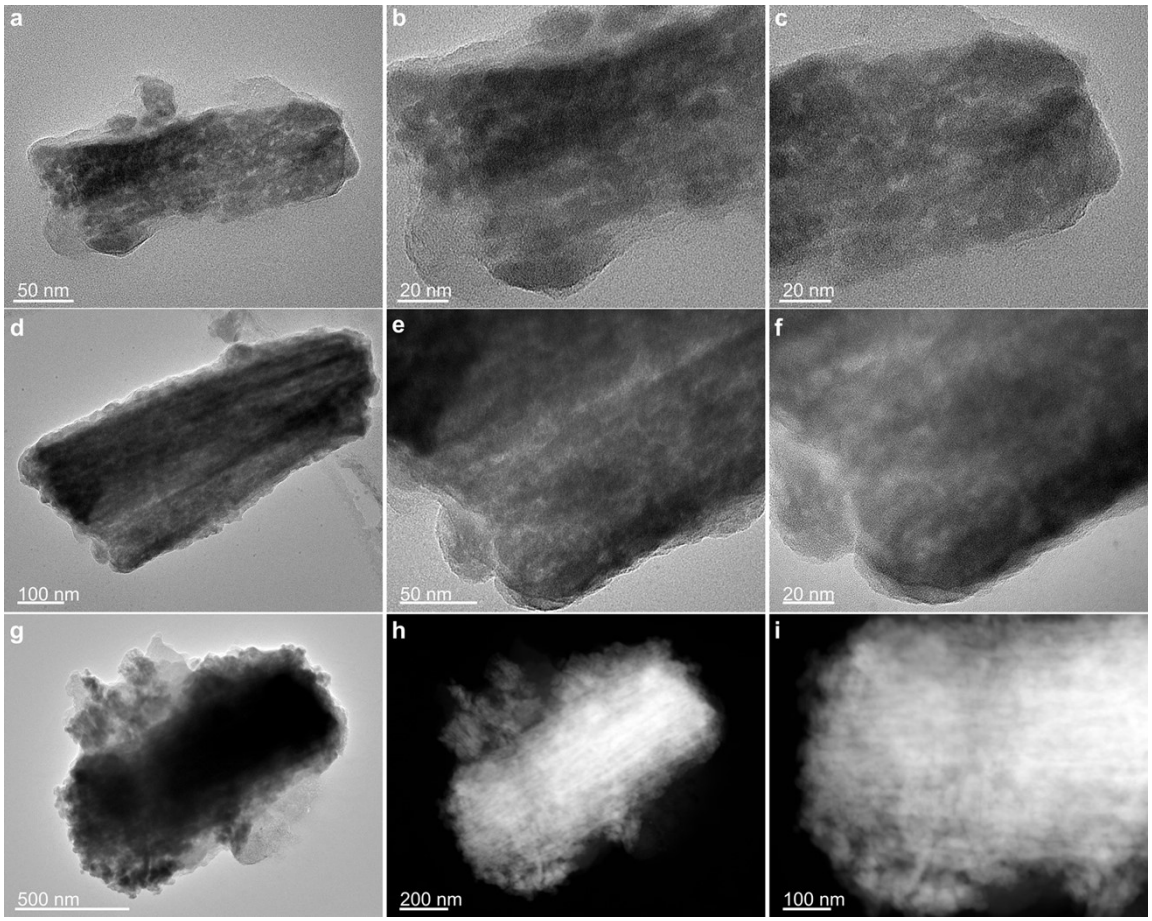

Fig. S19 TEM images for meso-Nb_2O_5@C: (a–f) at 0.5 C after 100 cycles. (g–i) at 20 C after 10,000 cycles.

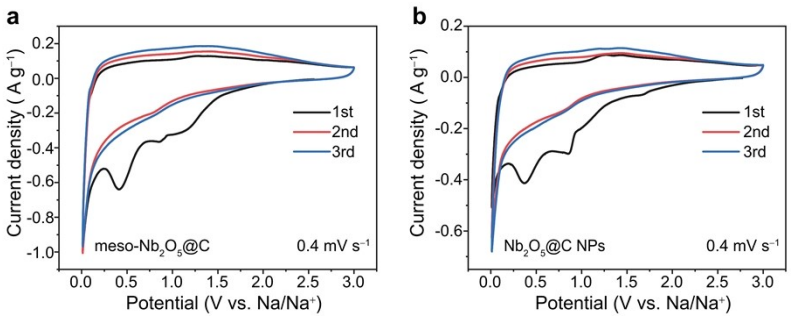

Fig. S20 CVs with different cycles at 0.4 mV s^{-1} of the meso-Nb_2O_5@C electrodes (a) and the Nb_2O_5@C NP electrodes (b), respectively.

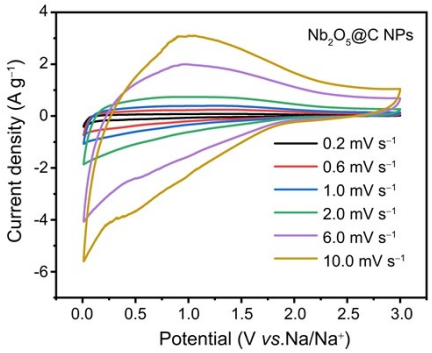

Fig. S21 CV curves of the Nb_2O_5@C NPs electrodes at different scan rates.

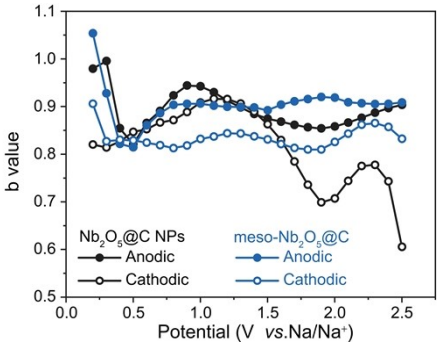

Fig. S22 Corresponding *b* values for meso-Nb_2O_5@C and Nb_2O_5@C NPs at various potentials.

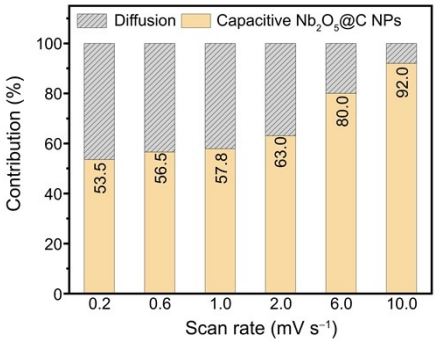

Fig. S23 The capacitive contributions for Nb_2O_5@C NPs at various scan rates.

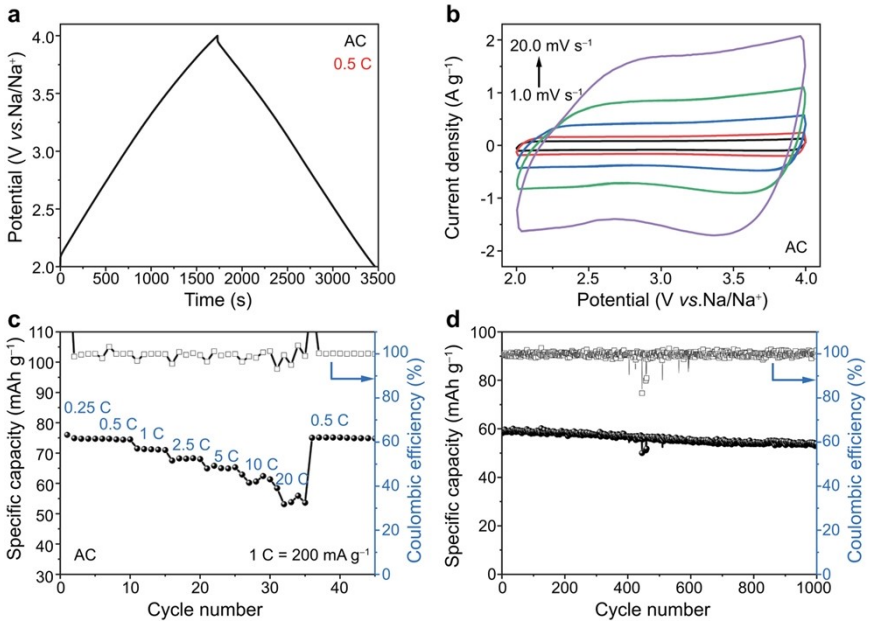

Fig. S24 Electrochemical performance for AC electrode: (a) galvanostatic discharge/charge voltage profiles at 0.5 C. (b) CV curves at different scan rates. (c) rate performance. (d) cycling performance at 5 C.

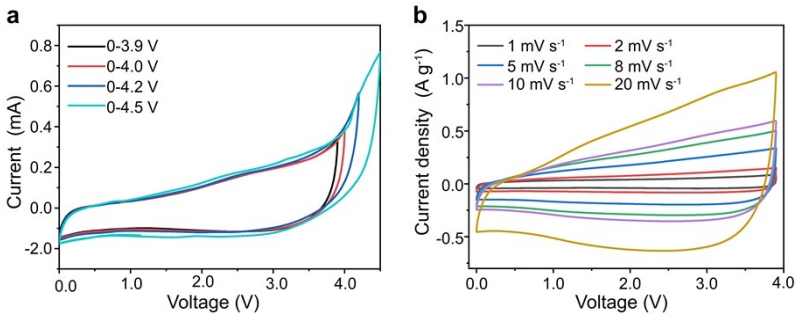

Fig. S25 CV curves for for meso-Nb_2O_5@C//AC SIC: (a) CV curves in different voltage ranges at 5 mV s^{-1}; (b) CV curves at different scan rates .

Table S1 Different microwave reaction time

Sample Name	Precursor Solution			Micro-heating Time
	ammonium niobate (V) oxalate hydrate	OA	TOA	
1 min	0.4 g	5 mL	16 mL	1 min
10 min				10 min
30 min				30 min

Table S2. Specific surface area for samples with different microwave reaction

Sample	1 min	10 min	30 min
BET surface area	47.3 m^2 g^{-1}	25.6 m^2 g^{-1}	46.6 m^2 g^{-1}

Table S3 Different concentration for Nb^{5+} source

Sample Name	Precursor Solution			Micro-heating Time
	ammonium niobate (V) oxalate hydrate	OA	TOA	
0.1 g	0.1 g	5 mL	16 mL	1 min
0.2 g	0.2 g			
0.3 g	0.3 g			
0.4 g	0.4 g			
0.5 g	0.5 g			

Table S4 Different ratios of OA to TOA

Sample	Precursor Solution			Micro-heating
Name	ammonium niobate (V) oxalate hydrate	OA	TOA	Time
0 mL OA	0.4 g	0 mL	21 mL	1 min
5 mL OA		5 mL	16 mL	
10 mL OA		10 mL	11 mL	
16 mL OA		16 mL	5 mL	
pure OA		21 mL	0 mL	

Table S5. Comparison of the specific surface area

Sample	Nb_2O_5@C NPs	Meso-Nb_2O_5@C
BET surface area	42.6 $m^2 g^{-1}$	47.3 $m^2 g^{-1}$

Table S6. The relative value for equivalent circuit for meso-Nb_2O_5 and Nb_2O_5@C NPs

Electrode State	material	R_Ω (Ω)	R_{ct} (Ω)	Z_w (Ω)
Before cycles	meso-Nb_2O_5@C	5.7	234.1	650.6
	Nb_2O_5@C NPs	4.6	249	751.4
After cycles	meso-Nb_2O_5@C	7.1	278.7	466.7
	Nb_2O_5@C NPs	5.4	302.8	1058

Supplementary References

[1] Y. Qiao; X. Hu; Y. Liu; C. Chen; H. Xu; D. Hou; P. Hu; Y. Huang, *J. Mater. Chem. A* 2013**, 1**, 10375–10381.

[2] L. Zhang; J. Sun; H. Zhao; Y. Sun; L. Dai; F. Yao; Y. Fu; J. Zhu, *J. Power Sources* 2020**, 475**, 228679–228688.

[3] L. Wang; H. Yang; T. Shu; Y. Xin; X. Chen; Y. Li; H. Li; X. Hu, *ACS Appl. Energy Mater.* 2018**, 1**, 1708-1715.

[4] K. Saito; A. Kudo, *Dalton Trans* 2013**, 42**, 6867-6872.

[5] T. Andelman; Y. Gong; M. Polking; M. Yin; I. Kuskovsky; G. Neumark; S. O'Brien, *J Phys Chem B* 2005**, 109**, 14314-14318.